Mesh-free methods for transient heat conduction

Vladimir Sladek[1]*, Jan Sladek[1] and Chuanzeng Zhang[2]

[1]*Institute of Construction and Architecture, Slovak Academy of Sciences*
845 03 Bratislava, Slovakia
e-mail: vladimir.sladek@savba.sk

[2]*Department of Civil Engineering, University of Siegen,*
Paul-Bonatz-str.9-11, D-57076 Siegen, Germany
e-mail: c.zhang@uni-siegen.de

Abstract

The paper deals with transient heat conduction in functionally gradient materials. The spatial variation of the temperature field is approximated by using alternatively two various mesh free approximations, while the time dependence is treated either by the Laplace transform method and/or by the polynomial interpolation in the time stepping method. The accuracy and convergence of the numerical results as well as the computational efficiency of various approaches are compared in numerical test example.

Keywords: heat transfer, boundary value problems, numerical analysis, integral equations, meshless methods

1. Introduction

In two last decades, the mesh-free methods became popular in various branches of computational physics and engineering because of avoiding certain inappropriateness of discretization techniques based on elements (generation of meshes, remeshing, large distortions of elements, separation of continua, etc). Another important aspect followed in this paper is the local integral equation (LIE) formulation reflecting the integral form of the physical balance principles. The LIE combined with mesh-free approximations enables us to develop completely element-free formulations. Since no fundamental solutions are employed, the formulations are quite general without any restrictions e.g. due to material non-homogeneities.

It is well known that the shape functions in mesh-free approximations are not available in closed form and certain computational procedure must run for getting them. This handicap yields prolongation of the computational time what is mainly criticized. Fortunately, this disadvantage can be overcome by using local weak formulation with analytical integration. In such a formulation, however, higher-order derivatives are required. Since the accuracy of such derivatives calculated by standard differentiation is not satisfactory, especially near the boundary of the analyzed domain, modified differentiation is more appropriate. As regards the treatment of time variations in transient problems, the Laplace transform and time-stepping techniques belong to most frequently used. Note that in the case of higher-order time interpolations a correct treatment of the discretized governing equation for the first time instant is required.

2. Governing equations. Differential and integral fromulations

The equation for transient heat conduction in isotropic and continuously non-homogeneous media is given by the partial differential equation of parabolic type with variable coefficients [10]

$$\left(\lambda(\mathbf{x})u_{,k}(\mathbf{x},t)\right)_{,k} - \rho(\mathbf{x})c(\mathbf{x})\frac{\partial u(\mathbf{x},t)}{\partial t} = -w(\mathbf{x},t)\,, \tag{1}$$

in $\Omega\times[0,T]$, where $u(\mathbf{x},t)$ is the temperature field, $w(\mathbf{x},t)$ is the volume density of heat sources (for diffusion problems $w=0$), $\rho(\mathbf{x})$ is the mass density, $c(\mathbf{x})$ is the volume density of the specific heat per unit mass, and $\lambda(\mathbf{x})$ is the thermal conductivity coefficient. The first term on the left-hand side of Eq.(1) is the divergence of the heat flux vector

$$q_k(\mathbf{x},t) = -\lambda(\mathbf{x})u_{,k}(\mathbf{x},t) \tag{2}$$

and the second term is the rate of the temporal change of the volumetric density of heat. The physically reasonable boundary conditions of the problem can be classified as the Dirichlet, Neumann and Robin b.c.

The boundary conditions are to be supplemented by the initial condition, which in the present parabolic problem is the initial value of the temperature

$$u(\mathbf{x},0) = v(\mathbf{x}) \quad \text{in} \quad \Omega\cup\partial\Omega\,. \tag{3}$$

The governing equation in differential form (1) is derived form the physical balance principles which take an integral form in a continuum theory. Let us consider an arbitrary piece of continuum contained in a domain Ω^c bounded with the boundary $\partial\Omega^c$. Then, the energy balance for a considered continuum is expressed as

$$\int_{\partial\Omega^c} n_i(\boldsymbol{\eta})q_i(\boldsymbol{\eta},t)d\Gamma(\boldsymbol{\eta}) + \int_{\Omega^c}\rho(\mathbf{x})c(\mathbf{x})\frac{\partial}{\partial t}u(\mathbf{x},t)d\Omega(\mathbf{x}) = \int_{\Omega^c} w(\mathbf{x},t)d\Omega(\mathbf{x}) \tag{4}$$

In view of the Gauss divergence theorem, one can see that Eq. (4) is an equivalent of Eq. (1) since each of them can be

* This article has been produced with the financial assistance of the European Regional Development Fund (ERDF) under the Operational Programme Research and Development/Measure 4.1 Support of networks of excellence in research and development as the pillars of regional development and support to international cooperation in Bratislava region/Project No. 26240120020 Building the centre of excellence for research and development of structural composite materials – 2nd stage.
This work has been partially supported by the Slovak Science and Technology Assistance Agency registered under number APVV-0032-10 and the Slovak Grant Agency VEGA-2/0039/09, which are gratefully acknowledged.

derived from the other one under the assumption of arbitrary choice of the sub-domain $\Omega^c \subset \Omega$.

Sometimes, the time evolution is investigated by using the Laplace transformation. Then, the governing equations (1) and/or (4) can be rewritten for the Laplace transform of the temperature $\overline{u}(\mathbf{x}, p)$ as

$$\left(\lambda(\mathbf{x})\overline{u}_{,k}(\mathbf{x}, p)\right)_{,k} - p\rho(\mathbf{x})c(\mathbf{x})\overline{u}(\mathbf{x}, p) = \\ = -\overline{w}(\mathbf{x}, p) - \rho(\mathbf{x})c(\mathbf{x})v(\mathbf{x}) \tag{5}$$

$$\int_{\partial\Omega^c} n_i(\boldsymbol{\eta})\lambda(\boldsymbol{\eta})\overline{u}_{,i}(\boldsymbol{\eta}, p)d\Gamma(\boldsymbol{\eta}) - p\int_{\Omega^c} \rho(\mathbf{x})c(\mathbf{x})\overline{u}(\mathbf{x}, p)d\Omega(\mathbf{x}) = \\ = -\int_{\Omega^c} \left[\overline{w}(\mathbf{x}, p) + \rho(\mathbf{x})c(\mathbf{x})v(\mathbf{x})\right]d\Omega(\mathbf{x}). \tag{6}$$

For the Laplace-inversion algorithms we shall use the Stehfest's algorithm [8] with ten values of the transform parameter for each time instant.

3. Spatial approximations.

The spatial variations of the field variables will be approximated by using either the Central Approximation Node (CAN) concept of the Moving Least Squares approximation (MLS) or the Point interpolation method (PIM). Both of them yield mesh-free implementations since no predefined connectivity among nodal points is required [5].

3.1. MLS-approximation

In the MLS-approximation, the polynomial basis is employed and the expansion coefficients are found from minimization of weighted squares of residua at a finite number of nodal points [1]. Let $\mathbf{x}^q$ be the CAN for the approximation at a point $\mathbf{x}$. Then, the amount of nodes involved into the approximation at $\mathbf{x}$ is reduced a-priori from N_t (total number of nodes) to N^q, where N^q is the number of nodes supporting the approximation at the CAN $\mathbf{x}^q$, i.e. the amount of nodes in the set $\mathcal{M}^q = \left\{\forall \mathbf{x}^a;\, w^a(\mathbf{x}^q) > 0\right\}_{a=1}^{N_t}$, where $w^a(\mathbf{x})$ is the weight function associated with the node $\mathbf{x}^a$ at the field point $\mathbf{x}$. In this paper, we employ the Gaussian weights [5]. The MLS-CAN approximation for spatial variation of the field variable $f(\mathbf{x}) \in \{u(\mathbf{x}, t), \overline{u}(\mathbf{x}, p)\}$ can be expressed in terms of nodal unknowns $\hat{f}^{n(q,a)}$ and shape functions $\phi^{n(q,a)}(\mathbf{x})$

$$f(\mathbf{x}) \approx \sum_{a=1}^{N^q} \hat{f}^{n(q,a)}\phi^{n(q,a)}(\mathbf{x}), \tag{7}$$

where $n(q,a)$ is the global number of the a-th local node from $\mathcal{M}^q$, $\hat{f}^{n(q,a)} \in \{\hat{u}^{n(q,a)}(t), \hat{\overline{u}}^{n(q,a)}(p)\}$. In this paper, we shall specify the CAN $\mathbf{x}^q$ as the nearest node to the approximation point $\mathbf{x}$. Recall that the nodal unknowns are different from the nodal values of physical quantities, in general. Furthermore, the shape functions $\phi^m(\mathbf{x})$ are not known in closed form and a computational procedure must run for evaluation at each approximation point $\mathbf{x}$. This is the main handicap of mesh-free approximations as compared with mesh-based approximations utilizing mostly polynomial interpolations.

3.2. Point interpolation method

In the case of PIM, the basis functions are taken as a combination of polynomials and radial basis functions (RBF) [2]. Then, one can solve the problem of accuracy and numerical stability of the approximation [2, 5]. In this paper, we shall consider ten polynomials (the complete set of polynomials up to the third order) and the RBFs will be taken as multiquadrics

$$R^n(\mathbf{x}) = \left(\left|\mathbf{x} - \mathbf{x}^n\right|^2 + (c^n)^2\right)^{m/2} \quad \text{with } m = 7,$$

and for the shape parameter c^a we choose h^a which is the minimal distance from $\mathbf{x}^a$ to other nodes.

Formally, the approximation can be expressed by (7), i.e. it is the same as in the MLS-approximation, but now the nodal unknowns are directly the values of the approximated field variable, since the shape functions obey the Kronecker–delta property.

3.3. Approximation of field derivatives

Besides the approximation of field variables, we need also their gradients which can be approximated as gradients of approximated fields (7)

$$f_{,j}(\mathbf{x}) \approx \sum_{a=1}^{N^q} \hat{f}^{n(q,a)}\phi_{,j}^{n(q,a)}(\mathbf{x}) \tag{8}$$

and similarly, one can approximate also higher-order derivatives in this *standard differentiation* (*sdif*) approach. Recall that the evaluation of the derivatives of the shape functions is still more complicated than the evaluation of shape functions and also the accuracy of such approximations is worse especially near the boundary of the analyzed domain.

In order to facilitate the evaluation of higher-order derivatives, the *modified differentiation* (*mdif*) approach has been proposed [4, 9, 6]. In the *mdif* approach, the higher order derivatives of the potential field are expressed in terms of the first order derivatives of the shape functions $F_k^{qa} = \phi_{,k}^{n(q,a)}(\mathbf{x}^q)$ and the nodal values $\hat{f}^{n(q,a)}$ using the recurrent formula

$$f_{,ij\ldots k}^{(r)}(\mathbf{x}^q) \approx \sum_{a=1}^{N^q} f_{,ij\ldots}^{(r-1)}(\mathbf{x}^{n(q,a)})\phi_{,k}^{n(q,a)}(\mathbf{x}^q), \tag{9}$$

where the nodal values of the $(r-1)$ order derivatives and the first order derivatives of the shape functions are used for approximation of the r order derivative of displacements with

$$f^{(0)}(\mathbf{x}^{n(q,a)}) = \hat{f}^{n(q,a)}. \tag{10}$$

Thus, for the second and third order derivatives we have

$$f_{,jk}(\mathbf{x}^c) = \underset{jk}{sym}\left\{\sum_{a=1}^{N^c} F_k^{ca} \sum_{\substack{b=1 \\ v=n(c,a)}}^{N^v} F_j^{vb}\hat{f}^{n(v,b)}\right\} \tag{11}$$

$$f_{,jil}(\mathbf{x}^c) = \underset{jil}{sym}\left\{\sum_{a=1}^{N^c} F_l^{ca} \sum_{\substack{b=1 \\ v=n(c,a)}}^{N^v} F_i^{vb} \sum_{\substack{d=1 \\ w=n(v,b)}}^{N^w} F_j^{wd}\hat{f}^{n(v,b)}\right\} \tag{12}$$

where symmetrization is assumed with respect to the indicated indices. Eqs. (11) and (12) can be simplified as

$$f_{,jk}(\mathbf{x}^c) = \sum_{a=1}^{M^c} F_{jk}^{ca}\, \hat{f}^{m(c,a)} \tag{11*}$$

$$f_{,jil}(\mathbf{x}^c) = \sum_{a=1}^{K^c} F_{jil}^{ca}\, \hat{f}^{k(c,a)} \tag{12*}$$

where the global numbers $m(c,a)$ as well as M^c and F_{jk}^{ca} can be obtained from comparison of Eqs. (11) and (11*). Similarly from (12) and (12*), one can find $k(c,a)$, K^c and F_{ljk}^{ca}. The further extension for higher-order derivatives is straightforward. The higher-order derivatives are required either in the strong formulation or in the weak formulation utilizing the analytical integrations.

3.4. Spatially discretized governing equations

Substituting the spatial approximations into the governing equations (5) and/or (6) considered at nodal points $\mathbf{x}^c$ (Ω^c э $\mathbf{x}^c$ is a sub-domain around the node $\mathbf{x}^c$), one obtains the system of algebraic equations

$$\sum_g \left(K^{cg} - p_n M^{cg} \right) \hat{\bar{u}}^g(p_n) = -\,\bar{R}^c(p_n), \quad (c = 1,2,...,N_t), \tag{13}$$

which should be solved for each value of the transform parameter p_n ($n = 1,2,...,N$; $N = 10$ in this paper).

The matrix elements are given as

$$\begin{aligned} K^{cg} &= \lambda(\mathbf{x}^c)\phi^g_{,kk}(\mathbf{x}^c) + \lambda_{,k}(\mathbf{x}^c)\phi^g_{,k}(\mathbf{x}^c), \\ M^{cg} &= \rho(\mathbf{x}^c)c(\mathbf{x}^c)\phi^g(\mathbf{x}^c), \\ \bar{R}^c(p_n) &= \bar{w}(\mathbf{x}^c, p_n) + \rho(\mathbf{x}^c)c(\mathbf{x}^c)v(\mathbf{x}^c), \end{aligned} \tag{14}$$

$g = n(c,a)$ with $a \in \mathcal{M}^c$

for the strong formulation (i.e. discretization of the governing PDE) which will be referred as the CPDE approach (collocation of PDE), while in the case of weak formulation starting from Eq. (6), the matrix elements are given as

$$\begin{aligned} K^{cg} &= \int_{\partial\Omega^c} n_i(\boldsymbol{\eta})\lambda(\boldsymbol{\eta})\phi^{n(q_\eta,a)}_{,i}(\boldsymbol{\eta})d\Gamma(\boldsymbol{\eta}), \\ M^{cg} &= \int_{\Omega^c} \rho(\mathbf{x})c(\mathbf{x})\phi^{n(q_x,a)}(\mathbf{x})d\Omega(\mathbf{x}), \\ \bar{R}^c(p_n) &= \int_{\Omega^c} \left[\bar{w}(\mathbf{x}, p_n) + \rho(\mathbf{x})c(\mathbf{x})v(\mathbf{x})\right] d\Omega(\mathbf{x}), \end{aligned} \tag{15}$$

with g being global numbers of nodes generated by $n(q_\eta, a)$ and/or $n(q_x, a)$, where q_x is the nearest nodal point to the integration point $\mathbf{x}$.

Similarly, substituting the approximations for the temperature and its gradients into the governing equations (1) and/or (4), we obtain the system of the ordinary differential equations (semi-discretized governing equations)

$$\sum_g \left(K^{cg}\hat{u}^g(t) - M^{cg}\frac{\partial \hat{u}^g(t)}{\partial t} \right) = -\,R^c(t), \quad (c = 1,2,...,N_t), \tag{16}$$

with $R^c(t) = w(\mathbf{x}^c, t)$ in the strong formulation, while $R^c(t) = \int_{\Omega^c} w(\mathbf{x},t)d\Omega(\mathbf{x})$ in the weak formulation.

3.5. Weak formulation with analytical integrations

From comparison of the matrix elements (14) and (15), one can see immediately that in the strong formulation it is sufficient to evaluate the shape functions and their derivatives at collocation points while in the in the weak formulation these must be computed at each integration point what results in enormous prolongation of the time needed for creation of the system matrix. Another difference is that in the matrix elements K^{cg} only the first derivatives of the shape functions are required. In order to reduce the amount of points at which the shape function derivatives are to be evaluated, one can accomplish the integration in a closed form under certain assumptions [7]. For this purpose, we shall assume the circular sub-domains centred at nodes $\mathbf{x}^c$. Furthermore, the radius of the circle r_o is taken sufficiently small, in order to justify the Taylor series expansion of the material coefficients as well as the shape functions within the sub-domain. If the material coefficients are prescribed by analytical functions, there is no basic problem to calculate their derivatives at nodal points. Expecting failure of accuracy of higher order derivatives of the shape functions, the size of the radius of sub-domains should guarantee fast convergence of the Taylor series expansion. Assuming the mass density to be constant and the Taylor series expansions up to 4th orders for material parameters and the shape functions with neglecting the terms $O(r_o^6)$, one obtains

$$\begin{aligned} &\frac{1}{\pi r_o^2}\int_{\partial\Omega^c} n_i(\mathbf{x})\lambda(\mathbf{x})u_{,i}(\mathbf{x},t)d\Gamma \approx \Lambda_i^{1c}u_{,i}(\mathbf{x}^c,t) + \\ &+\Lambda_{ip}^{2c}u_{,ip}(\mathbf{x}^c,t) + \Lambda_{ips}^{3c}u_{,ips}(\mathbf{x}^c,t) + \Lambda_{ipkf}^{4c}u_{,ipkf}(\mathbf{x}^c,t) \end{aligned} \tag{17}$$

$$\begin{aligned} &\frac{\rho}{\pi r_o^2}\int_{\Omega^c} c(\mathbf{x})\frac{\partial}{\partial t}u(\mathbf{x},t)d\Omega(\mathbf{x}) \approx \rho\frac{\partial}{\partial t}\Big\{C^{0c}u(\mathbf{x}^c,t) + \\ &+C_p^{1c}u_{,p}(\mathbf{x}^c,t) + C_{ps}^{2c}u_{,ps}(\mathbf{x}^c,t) + C_p^{3c}u_{,pss}(\mathbf{x}^c,t) + \\ &+C^{4c}u_{,ppss}(\mathbf{x}^c,t)\Big\}, \end{aligned} \tag{18}$$

where $\Lambda_i^{1c} = \lambda_{,i}^c + \frac{r_o^2}{8}\lambda_{,imm}^c$

$$\begin{aligned} \Lambda_{ip}^{2c} &= \lambda^c\delta_{ip} + \frac{r_o^2}{8}\left(2\lambda_{,ip}^c + \lambda_{,jj}^c\delta_{ip}\right) + \frac{r_o^4}{24}\left(\frac{1}{2}\lambda_{,ipjj}^c + \frac{\delta_{ip}}{8}\lambda_{,ssjj}^c\right) \\ \Lambda_{ips}^{3c} &= \frac{r_o^2}{8}3\lambda_{,i}^c\delta_{ps} + \frac{r_o^4}{24}\left(\frac{3}{4}\lambda_{,ijj}^c\delta_{ps} + \frac{1}{2}\lambda_{,ips}^c\right) \\ \Lambda_{ipkf}^{4c} &= \frac{r_o^2}{8}\lambda^c\delta_{ip}\delta_{kf} + \frac{r_o^4}{24}\left(\lambda_{,ip}^c\delta_{kf} + \frac{1}{4}\lambda_{,jj}^c\delta_{ip}\delta_{kf}\right) \end{aligned} \tag{19}$$

$$C^{0c} = c^c + \frac{r_o^2}{8}c_{,pp}^c + \frac{r_o^4}{192}c_{,ppnn}^c$$

$$C_p^{1c}=\frac{r_o^2}{4}c_{,p}^c+\frac{r_o^4}{48}c_{,nnp}^c\ ,\qquad C_p^{3c}=\frac{r_o^4}{48}c_{,p}^c$$

$$C_{ps}^{2c}=\frac{r_o^2}{8}\left(c^c+\frac{r_o^2}{12}c_{,nn}^c\right)\delta_{ps}+\frac{r_o^4}{48}c_{,ps}^c\ ,\quad C_p^{4c}=\frac{r_o^4}{192}c^c\ . \quad (20)$$

Now, in view of Eqs. (8), (11)-(12*) and (17), (18), one obtains the matrix elements K^{cg} and M^{cg} for the weak formulation with analytical integration as

$$K^{cg}=\pi r_o^2\left\{\Lambda_i^{1c}\sum_{\substack{a=1\\ n(c,a)=g}}^{N^c}F_i^{ca}+\Lambda_{ip}^{2c}\sum_{\substack{a=1\\ m(c,a)=g}}^{M^c}F_{ip}^{ca}+\right.$$

$$\left.+\Lambda_{ips}^{3c}\sum_{\substack{a=1\\ k(c,a)=g}}^{K^c}F_{ips}^{ca}+\Lambda_{ipkf}^{4c}\sum_{\substack{a=1\\ l(c,a)=g}}^{L^c}F_{ipkf}^{ca}\right\} \quad (21)$$

$$M^{cg}=\rho\pi r_o^2\left\{\sum_{\substack{a=1\\ n(c,a)=g}}^{N^c}\left(C^{0c}\phi^{n(c,a)}(\mathbf{x}^c)+C_p^{1c}F_p^{ca}\right)+\right.$$

$$\left.+C_{ps}^{1c}\sum_{\substack{a=1\\ m(c,a)=g}}^{M^c}F_{ps}^{ca}+C_p^{3c}\sum_{\substack{a=1\\ k(c,a)=g}}^{K^c}F_{pps}^{ca}+C^{4c}\sum_{\substack{a=1\\ l(c,a)=g}}^{L^c}F_{ppss}^{ca}\right\} \quad (22)$$

It should be stressed that in contrast to Eq. (15) in expressions given by (21) and (22) the shape functions and their derivatives are required only at nodal points. Although the higher-order derivatives occur, they can be expressed in terms of the first order derivatives when the modified differentiation is employed. Note that the weak formulation with analytical integration (normalized by the area of sub-domain) converges to the strong formulation in the limit $r_o\to 0$. Moreover, the strong formulation corresponds to the lowest expansion terms in the weak formulation when the material coefficients and the shape functions derivatives are expanded into Taylor series. Hence, one can expect better accuracy by the weak formulation than by the CPDE approach especially for problems in considerably graded materials. Recall that the derived expressions for the matrix elements K^{cg} and M^{cg} are applicable for the weak formulation with analytical integration in both the time-stepping approach and the LT approach.

After the spatial discretization, the governing equations result into the semi-discrete ODE w.r.t. the time variable. In order to solve the ODE (16), we employ a polynomial interpolation for the time variation of the nodal unknowns.

4. Time interpolations.

The time interval $[0,T]$ is split by discrete time instants t_i into a finite number of subintervals

$$[0,T]=\bigcup_{i=0}^{m-1}[t_i,t_{i+1}],\quad \Delta t_i=t_{i+1}-t_i$$

Making use $n+1$ nodes, one can define element obeying interpolation of order n. We shall use either linear or quadratic Lagrange interpolation within time elements.

4.1. Linear Lagrange interpolation (LLI)

The element T_i is defined as the interval $T_i=[t_i,t_{i+1}]$ with the interior points being parametrized as

$$t\big|_{T_i}=\sum_{a=1}^{2}t_{i-1+a}N^a(\tau)=t_i+(1+\tau)\Delta t_i/2\ ,\quad \tau\in[-1,1] \quad (23)$$

since $N^1(\tau)=(1-\tau)/2$, $N^2(\tau)=(1+\tau)/2$.

The time dependence of a physical variable $u(t)$ is approximated on T_i by the interpolation

$$u(t)\big|_{T_i}=\sum_{a=1}^{2}u_{i-1+a}N^a(\tau)=\frac{1}{2}\left(u_{i+1}+u_i\right)+\frac{\tau}{2}\left(u_{i+1}-u_i\right) \quad (24)$$

with $u_k=u(t_k)$.

Then, the time derivative $\dot u(t)=du(t)/dt$ is approximated by the constant

$$\dot u(t)\big|_{T_i}=\frac{1}{J(\tau)}\frac{du}{d\tau}\bigg|_{T_i}=\frac{1}{\Delta t_i}\left(u_{i+1}-u_i\right)\ , \quad (25)$$

since the Jacobian of the transformation (23) is given as $J(\tau)=dt/d\tau\big|_{T_i}=\Delta t_i/2$.

Making use a different parametrization $\theta=(1+\tau)/2$ with $\theta\in[0,1]$, we obtain from (24) and (25)

$$u(t_i+\theta\Delta t_i)=\theta u_{i+1}+(1-\theta)u_i\ ,\ \dot u(t_i+\theta\Delta t_i)=\left(u_{i+1}-u_i\right)/\Delta t_i$$

Considering the system of the ODE (16) at $t=t_i+\theta\Delta t_i$, we obtain

$$\sum_g\left(K^{cg}-\frac{1}{\theta\Delta t_i}M^{cg}\right)\hat u_{i+1}^g=\sum_g\left((1-\frac{1}{\theta})K^{cg}-\frac{1}{\theta\Delta t_i}M^{cg}\right)\hat u_i^g$$

$$-\frac{1}{\theta}R^c(t_i+\theta\Delta t_i)\ ,\qquad (i=0,1,2,\dots) \quad (26)$$

which is the well known θ-method used in time stepping approaches for solution of the ODE with $\theta\in(0,1]$.

4.2. Quadratic Lagrange interpolation (QLI)

If we choose the time instants obeying $\Delta t_i=\alpha_i\Delta t$ with $\alpha_i\in\{1,2,3,\dots\}$, then it is easy to create also the higher order elements. Thus, for 3-node (quadratic) element T_i, the third node is t_{i+1}, the second node (mid-node) is t_i, and the first node is t_{i-k}, where k is found from the condition $\sum_{j=1}^{k}\alpha_{i-j}=\alpha_i$. Then, the interior points on T_i are parametrized as $t\big|_{T_i}=t_{i-k}N^1(\tau)+t_iN^2(\tau)+t_{i+1}N^3(\tau)=t_i+\tau\alpha_i\Delta t$, (27)

with $\tau\in[-1,1]$, since $N^1(\tau)=\tau(\tau-1)/2$, $N^2(\tau)=1-\tau^2$, $N^3(\tau)=\tau(\tau+1)/2$. A physical variable and its time derivative are approximated on T_i as

$$u(t)\big|_{T_i} = \frac{\tau}{2}(\tau-1)u_{i-k} + (1-\tau^2)u_i + \frac{\tau}{2}(\tau+1)u_{i+1} \quad , \tag{28}$$

$$\dot{u}(t)\big|_{T_i} = \frac{1}{J(\tau)}\frac{du}{d\tau}\bigg|_{T_i} = \frac{2\tau-1}{2\alpha_i\Delta t}u_{i-k} - \frac{2\tau}{\alpha_i\Delta t}u_i + \frac{2\tau+1}{2\alpha_i\Delta t}u_{i+1} \tag{29}$$

since the Jacobian of the transformation (27) is given by $J(\tau) = dt/d\tau\big|_{T_i} = \alpha_i\Delta t$.

Considering the system of the semi-discretized ODE (16) at the time instant $t = t_i + \theta\Delta t_i$, one can use directly the interpolation formulae (28) and (29) for $\tau = \theta \in [0,1]$. Then, we obtain the system of algebraic equations which can be solved subsequently for time instant unknowns $\hat{u}_{i+1}^g$, ($i = 1, 2, \ldots$)

$$\sum_g \left(K^{cg} - \frac{1}{\theta\alpha_i\Delta t}\frac{2\theta+1}{\theta+1}M^{cg} \right)\hat{u}_{i+1}^g = -\frac{2}{\theta(\theta+1)}R^c(t_i+\theta\Delta t_i) + \\ + \frac{1-\theta}{1+\theta}\sum_g K^{cg}\left(\hat{u}_{i-k}^g - 2(1+\frac{1}{\theta})\hat{u}_i^g\right) + \\ + \frac{1}{(\theta+1)\theta\alpha_i\Delta t}\sum_g M^{cg}\left((2\theta-1)\hat{u}_{i-k}^g - 4\theta\hat{u}_i^g\right). \tag{30}$$

This sequence of equation systems should be supplemented with equations for unknowns $\hat{u}_1^g$. Eq. (30) is valid also for $i = 0$, but it involves also the nodal unknown at fictitious time instant. For this purpose, we assume that the first node on T_1 is taken at fictitious time instant $t_{-1} = t_0 - \Delta t_0$. Then, from (29) at t_0 (i.e., $i = 0$ and $\tau = 0$), we have

$$\hat{u}_{-1}^g = \hat{u}_1^g - 2\Delta t_0\dot{\hat{u}}^g(t_0) \quad . \tag{31}$$

Furthermore, from (16), we have

$$\dot{\hat{u}}_0^g = S^g + \sum_{g'} D^{gg'}\hat{u}_0^{g'} \quad , \quad D^{gg'} = \sum_{a=1}^{N_t}(M^{-1})^{ga}K^{ag'} \quad ,$$

$$S^g = \sum_{a=1}^{N_t}(M^{-1})^{ga}R^a(t_0) \tag{32}$$

Hence after substituting (31) and (32) into (30) at $i = 0$, we obtain

$$\sum_g \left(K^{cg} - \frac{2}{\theta\Delta t_0}M^{cg} \right)\hat{u}_1^g = -\frac{1}{\theta^2}R^c(t_0+\theta\Delta t_0) - \\ -\frac{1}{\theta}\sum_g\left((1-\theta)\Delta t_0K^{cg} + (2-1/\theta)M^{cg}\right)S^g - \\ -\frac{1}{\theta}\sum_{g,g'}\left((1-\theta)\Delta t_0K^{cg} + (2-1/\theta)M^{cg}\right)D^{gg'}\hat{u}_0^{g'} - \\ -\frac{1}{\theta\Delta t_0}\sum_g\left((1/\theta-\theta)\Delta t_0K^{cg} + 2M^{cg}\right)\hat{u}_0^g \, . \tag{33}$$

Certain simplification of Eq. (33) takes place, if the initial temperature is uniformly distributed in the analyzed domain Ω . Then, $\sum_{g'} D^{gg'}\hat{u}_0^{g'} = 0$, since $v(\mathbf{x}) = \text{const}$. The other simplifications occur in the right-hand sides of Eqs. (30) and (33), when the parameter $\theta = 1$ and/or $w(\mathbf{x},t) = 0$.

Note that the matrix elements K^{cg} and M^{cg} are independent of the time variable as well as the Laplace transform parameter. Nevertheless, their calculation in the weak formulation is time consuming because of lengthy evaluation of shape functions and their derivatives at integration points. This handicap can be eliminated by using the weak formulation with analytical integration as discussed above. For comparison of efficiency of the LT and the time stepping approaches recall that the former approach requires computation of the set of nodal unknowns for several values of the Laplace parameter for each considered time instant, while the later approach needs computation of the set of nodal unknowns at each time instant before the considered time instant.

5. Numerical tests and conclusions.

In order to study the accuracy and convergence of numerical results, we shall consider the example for which the exact solution is available [3]. In this paper, we consider a square domain $L \times L$ occupied by medium with exponentially graded heat conduction as well as specific heat while constant mass density: $\rho = \text{const}$., $\lambda(\mathbf{x}) = \lambda_0 \exp(2\delta x_2/L) = c(\mathbf{x})\lambda_0/c_0$. The constant values of the temperature are prescribed on the bottom u_0 and top u_L of the square, while the lateral sides are thermally insulated for $t \in [0, T]$ and constant initial value of temperature $v(\mathbf{x}) = \text{const} = v$ is assumed. In numerical computations, we have used $\lambda_0 = 1 = c_0 = \rho$, $\delta = 1$, $u_0 = 1 = v$, $u_L = 20$. The uniform distribution of nodal points is employed with h being the distance between two neighbour nodes.

Rather good accuracy is achieved for derivatives of the temperature at interior points, but it fails near the boundary of the analyzed domain especially for the third and higher orders derivatives. Fig. 1 shows the convergence of the third order derivatives on the top of the square domain by using the standard and modified differentiation techniques with assuming the nodal values of the temperature either prescribed or computed by solving the boundary value problem. According to this study, we have used the modified differentiation in what follows.

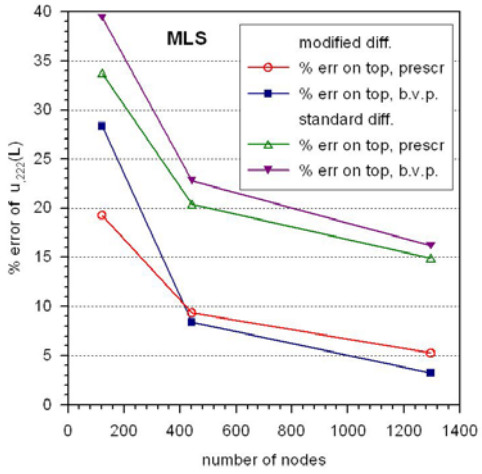

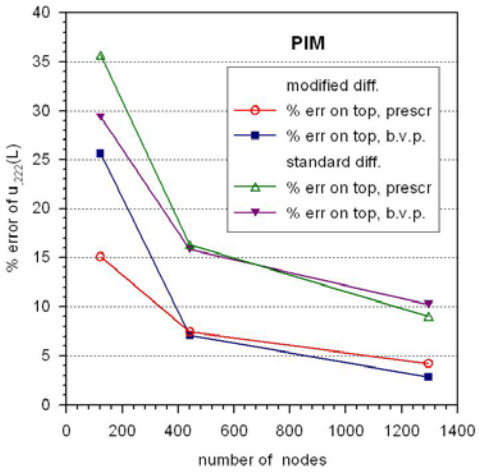

Figure 1: Convergence study for the third order derivatives

All of the tested computational techniques [CPDE – strong formulation; weak formulations: LIE(ni) – Local Integral Equations with numerical integration and LIE(ai) – LIE with analytical integration; all combined with the LT-technique as well as time-stepping techniques] give acceptable results at points sufficiently far from the boundary and at later time instants after sudden thermal loading.

In order to demonstrate the spatial and temporal localization of computational errors, we present the results by LIE(ai)

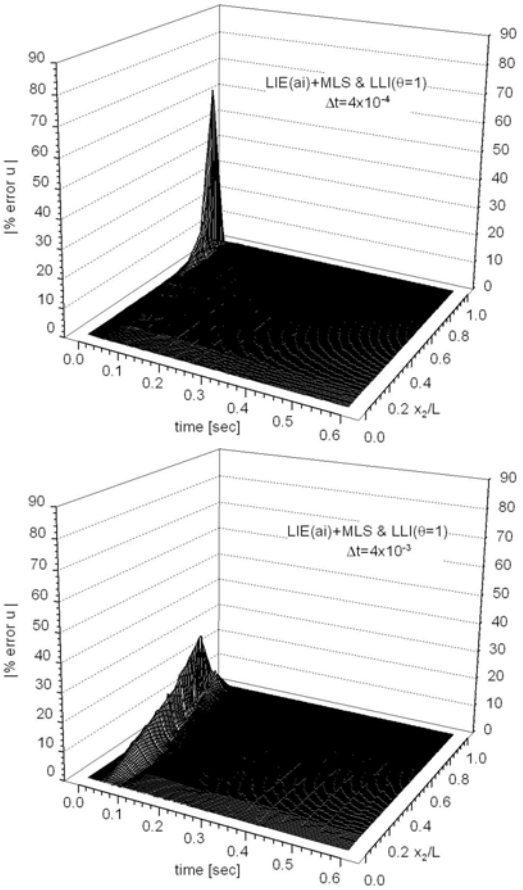

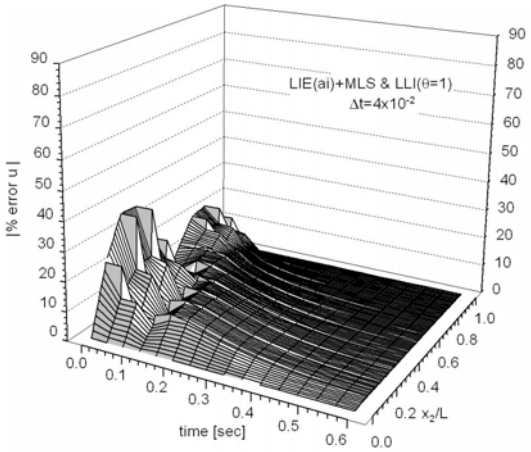

It can be seen from Fig.2 that considerable errors are sharply localized in both the space and time for short time steps. The inaccuracy of the numerical results by the LLI approach is partially decreased and remarkably delocalized with increasing the time step, while in the case of LT approach the delocalization is marginal as compared to the substantial increase of accuracy. For more detailed study of errors near the top side of the analyzed domain, we have used 1296 nodes and the test point is $(L/2,\ 0.9L)$.

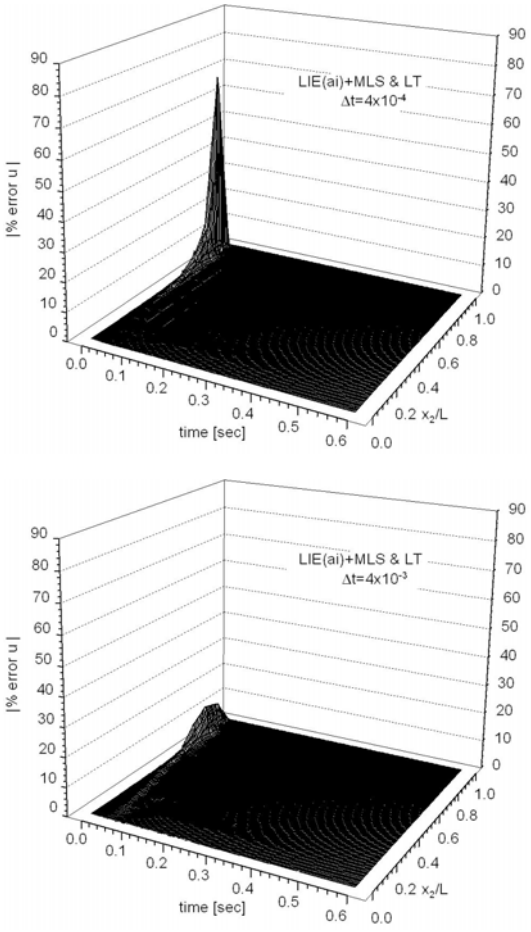

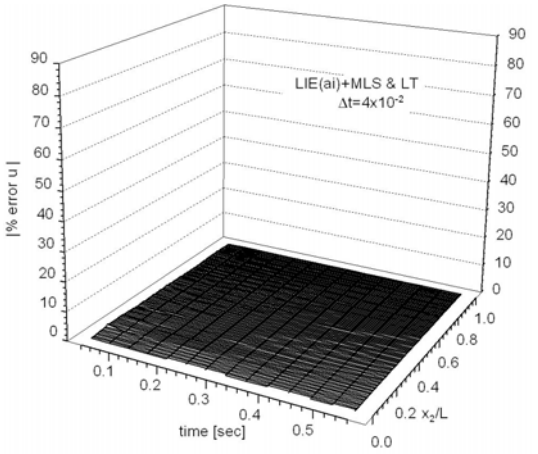

Figure 2: Evolutions of error distributions by LLI and LT approaches using 121 nodes in LIE(ai)+MLS and various time steps Δt

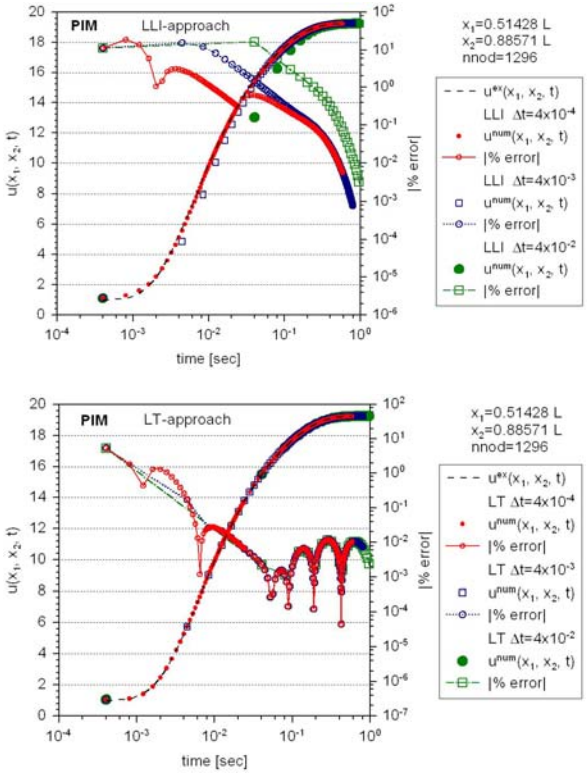

Figure 3: Time distribution of % errors for numerical results near the top of square domain by LLI and LT approaches using 1296 nodes in LIE(ai)+PIM and various time steps Δt

Fig. 3 shows the numerical results at the point (x_1, x_2) which is the nearest node to the point $(L/2,\ 0.9L)$. The sequences of time instants at which the numerical results are received are given as follows: $t_i = 4\times10^{-4} + (i-1)\Delta t$, $(i = 1, 2, ...)$ for three different time steps Δt. Thus, the time step is used for specification of time instants in the calculations by both the LT approach and LLI approach, but in the latter one, the time step is also the length of the time interval within which the interpolation is assumed. Recall that the prescribed boundary temperature $u_L = 20$ represents a sudden change at $t = 0$ with respect to the initial value of temperature $v = 1 = u_0$. It can be seen that better accuracy is achieved by the LT approach especially when the longer time steps are employed.

Note that three characteristic lengths play a role in this fully discretized transient field problem:

(i) $l_h = h$ represents the distance between two neighbouring nodes

(ii) $l_S = R_i h$ represents the radius of the influence domain which is used for selection of nodes contributing to the meshless approximation at certain point

(iii) $l_T = \sqrt{(\lambda/\rho c)\Delta t}$ is the characteristic length corresponding to the time step Δt and represents the horizon reached by the heat conduction during the time step with respect to certain point.

In time stepping techniques, the optimal choice is $l_T \approx h$, because information at previous time instant t_{i-1} cannot reach the nearest neighbour node at t_i, if $l_T < h$; on the other hand, if $l_T > h$, information at a node and coming from the nearest neighbour node is not fresh.

Now, we can explain the inaccuracy of numerical results by both the LLI and LT approaches at several early time instants $t_i = i\Delta t \quad (i = 1, 2, ..., 5)$ if $\Delta t = 4\times10^{-4}$. In this case $l_T = 2\times10^{-2}$, hence the choice of 1296 uniformly distributed nodes is almost optimal. Then, $h = 1/(\sqrt{1296} - 1) = 0.02857$ and at early time instants, the prescribed boundary value $u_L = 20$ (which is different from the initial value $v = 1$) affects the approximation in the boundary layer $L - (l_T + l_S) < x_2 < L$ and hence also in the boundary layer $L - (l_T + l_S) < x_2 < L - l_T$, i.e. at points which lie behind the horizon of the heat conduction from the top of the analyzed domain. Quite different is the situation near the bottom of the analyzed domain, where the prescribed boundary value of the temperature is the same as its initial value $u_0 = v = 1$. With increasing Δt, l_T is increased and hence not only the time interval but also the boundary layer of inaccurate results by the time stepping approaches become wider.

On the other hand, in the case of the LT approach the solution at a time instant is independent of the time step and therefore the accuracy at the time instants $t_i = 4\times10^{-4} + (i-1)\Delta t_2$ (which occurs after $(i-1)$ steps $\Delta t_2 = 4\times10^{-2}$) is the same as the accuracy after $10\times(i-1)$ steps $\Delta t_3 = 4\times10^{-3}$ and/or after $100\times(i-1)$ steps $\Delta t_4 = 4\times10^{-4}$. These conclusions are confirmed by the numerical results presented in Fig.3.

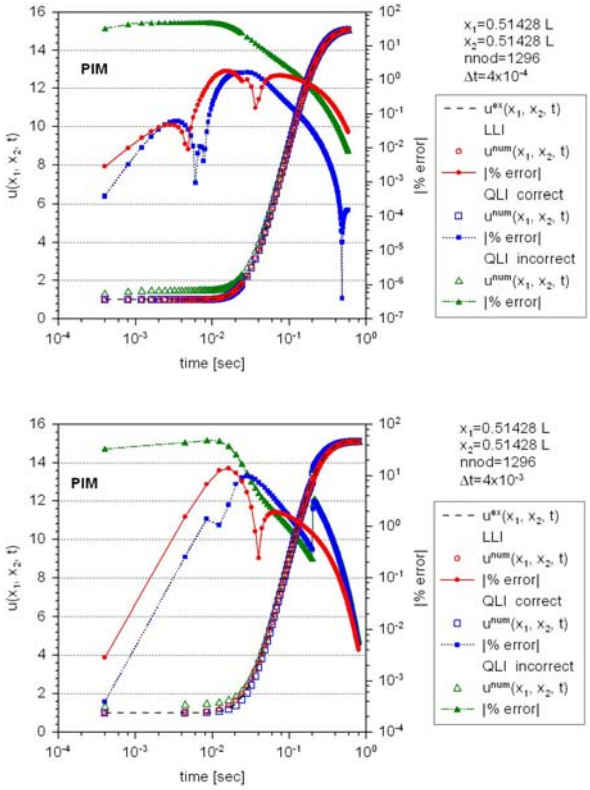

Figure 4: Time evolutions of temperatures and their accuracies by the LLI and two variants of QLI approaches at the node closest to the midpoint for two values of the time steps Δt

Finally, we present comparison of numerical results by the LIE(ai)+PIM combined with two variants of the QLI and LLI for time interpolations. In the correct variant of the QLI, Eq. (33) is employed at the first time instant, while in the incorrect variant Eq. (30) is utilized with neglecting the value $\hat{u}^g_{-1}$ at fictitious time instant. Recall that the assumption $\hat{u}^g_{-1} = 0$ is unjustified what is confirmed also by numerical results shown in Fig.4, where the incorrect QLI approach yields the error around 50% within rather wide time interval.

6. Conclusions

Both the strong and weak local formulations are proposed for solution of transient heat conduction in FGM. The spatial variation of temperature is approximated by using either the MLS approximation or the Point Interpolation method. In order to decrease the amount of evaluations of the shape functions and their derivatives, the local weak formulation with analytical integration is developed. This improves the computational efficiency, since the time needed for creation of the semi-discretized system matrix is decreased. The time dependence is treated either by the Laplace transform or by time-stepping techniques using either the linear or quadratic Lagrange interpolation. Both the LT and time-stepping approaches can give results with reasonable accuracy except very early time instants after sudden change of initial values by different prescribed boundary values. The time-stepping approach is sensitive to the choice of the time step, while the LT approach is stable. On the other hand, the computational economy is better in time-stepping approaches than in the LT approach if the solution is required not only at few time instants but within a time interval.

References

[1] Lancaster P. and Salkauskas K., Surfaces generated by moving least square methods, *Math. Comput*. 37, pp. 141-158, 1981.

[2] Liu G.R., *Mesh Free Methods, Moving Beyond the Finite Element Method*, CRC Press, Boca Raton, 2003.

[3] Sladek V., Sladek J., Tanaka M. and Zhang Ch., Transient heat conduction in anisotropic and functionally graded media by local integral equations, *Eng. Anal. Bound. Elem.* 29, pp. 1047-1065, 2005.

[4] Sladek V., Sladek J. and Zhang Ch., Analytical integrations in meshless implementations of local integral equations, *WCCM 8: Proceedings of the 8th World Congress on Computational Mechanics*, Schrefler B.A. and Perego U. Eds., CIMNE, Barcelona, CD –ROM, ISBN 978-84-96736-55-9, 2008.

[5] Sladek V., Sladek J. and Zhang Ch., Computation of stresses in non-homogeneous elastic solids by local integral equation method: a comparative study, *Comput. Mech*. 41, pp. 827-845, 2008.

[6] Sladek V., Sladek J. and Zhang Ch., Meshless implementations of local integral equations, *BEM/MRM 31: Mesh Reduction Methods*, Brebbia C.A. ed., WIT Press, Southampton, pp. 71-82, 2009.

[7] Sladek V. and Sladek J., Local integral equations implemented by MLS-approximation and analytical integrations, *Eng. Anal. Bound. Elem.* 34, pp. 904-913, 2010.

[8] Stehfest H., Algorithm 368: numerical inversion of Laplace transform, *Commun. Assoc. Comp. Machinery* 13, pp. 47-49, 624, 1970.

[9] Wen P.H. and Aliabadi M.H., An improved meshless collocation method for elastostatic and elastodynamic problems, *Commun. Numer. Meth. Engng*. 24, pp. 635-651, 2008.

[10] Wrobel L.C, *The Boundary Element Method, Vol. 1: Applications in Thermo-Fluids and Acoustic*, Wiley, Chichester, 2002.